Intracrystalline diffusion effects during *n*-alkane hydrocracking over Pt/H-ZSM5

Bart D.Vandegehuchte, Joris W. Thybaut and Guy B. Marin

Laboratory for Chemical Technology, Chemical Engineering Department, Ghent University, Krijgslaan 281-S5, Gent B-9000, Belgium

1. Introduction

A maximum efficiency of a catalyzed process is achieved by applying highly active materials which exhibit a maximum selectivity towards the desired reaction products. The latter constraint is often pursued by exploiting shape selective properties of catalysts built up from a specific pore network.[1,2] To this purpose, zeolite frameworks are ideally suited also because of their high hydrothermal stability and a typically high internal surface area.

Medium-pore ZSM5 catalysts are widely applied in bifunctional catalytic reactions such as hydroisomerization and hydrocracking of *n*-alkanes,[3-5] xylene isomerization,[6] and methane aromatization.[7] ZSM5 consists of elliptical straight channels (0.51 nmx 0.55nm) which are 1.0 nm long. They are perpendicularly crossed by zigzag channels (0.53 nm x 0.56 nm) with a circular cross section and a length of 1.2 nm. Cavities formed at the channel intersections have a diameter of about 0.85 nm.[3,8] For alkane hydroisomerization and –cracking, Experimental studies show that the effect of a narrower pore structure combined with the typical pore connectivity of a MFI framework results in a significant change in product selectivity in favor of the cracking products, compared to large-pore faujasites.[4,9,10]

Hydrocracking is a well-known refinery process which upgrades heavy residue oils to high-value middle distillates over metal-loaded acidic catalysts. On the metal phase, alkanes are first dehydrogenated into alkenes, the latter interacting much more strongly with the acid sites. Isomerization and cracking reactions typically take place after formation of an alkylcarbenium ion through protonation.[11] In case of non-shape-selective catalysts, the monobranched isomer product selectivities can be predicted from thermodynamic equilibrium considerations. In addition, the cracked product distribution is almost entirely determined from central-chain β-scission of highly reactive α,γ,γ-branched carbenium ions.[10]

The typical product distribution can be manipulated by using catalytic frameworks with other pore diameters and lattice connectivities. Whereas hydrocracking over faujasite-type zeolites resulted in the unconstrained reaction network described above,[11] the use of a beta zeolite which consists of a slightly narrower pore structure, already resulted in a significantly lower yield of ethyl-branched species.[12,13] Hydrocracking over a medium-pore ZSM22 zeolite which is built up from straight and narrow pore channels, mainly occurred at the pore mouths and resulted in a significant suppression of isomerization towards dibranched hydrocarbons.[10,14] In case of ZSM5, the pore diameter approaches the kinetic diameter of physisorbed alkanes. In addition with the typical channel configuration, mass transport limitations were found to be at the origin of the peculiar hydrocracking behavior of the catalyst,[4] even though some authors attributed transition state shape selectivity as a possible effect as well.[9,10] In case of multibranched species, the kinetic diameter exceeds the pore diameter which results in an near fixed position of dibranched species inside the catalyst framework, whereas from tribranched alkanes on, the sorbate is too bulky for formation inside the catalyst crystallite.[15,16] Both effects have their peculiar effect on the eventual cracked product distribution which, in case of ZSM5, is completely determined from β-scission of the immobile dibranched species.[17]

Besides its economic relevance, alkane hydrocracking is frequently applied for catalytic activity testing and model-guided catalyst design through optimization of so-called

'catalyst descriptors'.[18-21] A Single-Event MicroKinetic (SEMK) model is particularly suited for the latter endeavor as it is able to cope with large reaction networks through the assignment of elementary reaction families.[11,22,23] The methodology enables the calculation of a vast number of reaction rates via only a limited amount of kinetic parameters inherent to each reaction family. For a more detailed description of the single-event methodology is referred to Section 2.3. In this work, the SEMK model originally designed for alkane hydrocracking over an ultrastable Y zeolite is extended to incorporate simultaneous diffusion and reaction.[24] A methodology is worked out based on the Maxwell-Stefan (MS) theory applied to configurational diffusion in nanoporous materials by Krishna and Wesselingh.[25] Combined with the mean field approximation for MFI frameworks, worked out by Coppens et al.[26], diffusion of single components within a hydrocarbon sorbate mixture through a complicated nanoporous structure such as ZSM5, could be assessed from pure component self-diffusion coefficients at low occupancies only. Moreover, the model could easily be extended to other zeolite frameworks simply by adjusting the physisorption site connectivity rules corresponding with the zeolite unit cell. *n*-Hexane was chosen as first model component in order to eliminate the effect of the restricted formation of tribranched species. In a future step, the latter effect on the cracked product distribution is investigated by use of a *n*-octane hydrocracking data set.

2. Development of a model for simultaneous diffusion and reaction

2.1 Multi-component diffusion through a catalyst crystallite

Fick's law is commonly used for the description of mass transport induced by a concentration gradient:

$$J_i = -D_i \nabla c_i \tag{1}$$

With J_i the molar flux of component i in the mixture, and D_i the transport or Fick diffusivity. However, the transport diffusivity shows an irregular dependence on the mixture composition and partial pressure which complicates the description of multi-component diffusion through nanoporous materials via Fick's law.[27] To this purpose, the Maxwell-Stefan (MS) methodology is introduced which considers a force balance over each component within the reaction mixture.[25] The net force exhibited by each molecule is balanced by friction with the other diffusion species. E.g., for an ideal binary gas mixture of components i and j, the following relation is obtained:

$$-\frac{1}{c_i}\frac{\mathrm{d}p_i}{\mathrm{d}z} = -RT\frac{d\ln p_i}{dz} = -\frac{d\mu_i}{dz} \equiv \frac{RT}{\tilde{D}} x_j \left(u_j - u_i\right) \tag{2}$$

With p_i, μ_i and u_i the partial pressure, the chemical potential and the velocity of component i, respectively, and $\tilde{D}$ the MS diffusivity. $RT/\tilde{D}$ can be interpreted as the inverse of a drag coefficient which quantifies the drag force between the two moving species. Introduction of the thermodynamic correction factor Γ as a function of the activity coefficient γ of the corresponding component, a simple relation is found between the transport and the MS diffusivity which is often referred to as the Darken equation:

$$\Gamma_i = 1 + x_i \frac{\partial \ln \gamma_i}{\partial x_i} \tag{3}$$

$$D_i = \tilde{D}_i \Gamma_i \tag{4}$$

Γ quantifies the non-ideal behavior of the mixture and portrays the unpredictable nature of the transport diffusivity in case of highly non-ideal mixtures. The MS diffusivity is less affected by composition variations and, as already mentioned, can be physically interpreted as an inverse drag coefficient. Therefore, the MS diffusivity is generally preferred over the transport diffusivity. Extension to a multi-component mixture containing *n*

components, and accounting for the Gibbs-Duhem restriction for component *n*, results in a general expression for the (n-1)x1 **N** matrix containing the molar flux of each component.[25]

$$\mathbf{N} = -c_t \mathbf{B}^{-1} \boldsymbol{\Gamma} \nabla \mathbf{x} \tag{5}$$

With

$$B_{ii} = \frac{x_i}{\tilde{D}_{in}} + \sum_{\substack{k=1 \\ k\neq i}}^{n-1} \frac{x_k}{\tilde{D}_{ik}}, \qquad B_{ij(i\neq j)} = -x_i \left(\frac{1}{\tilde{D}_{ij}} - \frac{1}{\tilde{D}_{in}} \right), \qquad i,j = 1, 2, \ldots, n\text{-}1$$

$$\Gamma_{ij} = \delta_{ij} + x_i \frac{\partial \ln \gamma_i}{\partial x_i}, \qquad i, j = 1, 2, \ldots, n\text{-}1$$

Introducing a (n-1)x(n-1) matrix **D** containing the transport diffusivities, an analogous expression as Eqn. 4 can be derived in which the drag effects are decoupled from the thermodynamic effects:

$$\mathbf{D} = \mathbf{B}^{-1} \boldsymbol{\Gamma} \tag{6}$$

Extension towards multi-component diffusion in nanoporous materials comprises the incorporation of molecule-wall interactions besides intermolecular friction. Physisorption on the sorbent surface, however, dominates the diffusion mechanism in case of strong sorbate-sorbent interactions. The latter regime is often denoted as surface, intracrystalline, or configurational diffusion,[25] and is characterized by stronger pressure gradients, viscuous flow and steric effects. Simulation of configurational diffusion is performed via a mere extension of the 'dusty gas' model designed for combined bulk and Knudsen diffusion.[28] The vacant physisorption sites on the surface are considered as an immobile n+1th component in the MS equations (Eqn. 5). As a consequence, physisorption can be considered as a form of friction against mass transport over surfaces. The surface MS diffusivity is defined as:

$$\tilde{D}_i^{\mathrm{s}} = \frac{\tilde{D}_{i,n+1}^{\mathrm{s}}}{\theta_{n+1}} \tag{7}$$

Where θ_{n+1} is the fraction of vacant physisorption sites. $\tilde{D}_i^{\mathrm{s}}$ is also referred to as the corrected diffusivity and depends on the jump frequency which, in turn, is related to the site occupancy. The MS countersorption or interspecies diffusivity $\tilde{D}_{ij}^{\mathrm{s}}$ between components *i* and *j* is a measure for the facility at which component *j* is replaced by *i* at each physisorption site. The interspecies diffusivity at a given occupancy is approximated by the corrected diffusivities of the pure components at zero occupancy via an extension of the Vignes expression for diffusion in bulk liquid mixtures.[29]

$$\tilde{D}_{ij}^{\mathrm{s}} = \tilde{D}_{i,\theta=0}^{\mathrm{s}\,\frac{\theta_i}{\theta_i+\theta_j}} \tilde{D}_{j,\theta=0}^{\mathrm{s}\,\frac{\theta_j}{\theta_i+\theta_j}} \tag{8}$$

The corrected as well as the interspecies diffusivities depend strongly on the catalyst topology as well as on the site occupancy.[30] The corrected diffusivity follows an Arrhenius type relation with the activation barrier for diffusion.[31]

$$\tilde{D}^{\mathrm{s}} = A_D \exp\left(-\frac{E_{\mathrm{a},D}}{RT} \right) \tag{9}$$

2.2 Diffusion through a MFI unit cell

In this section, the mean field theory is introduced for the development of a relation between the corrected diffusivity of a sorbate molecule through a ZSM5 crystallite and the pure component self-diffusivity at low occupancy. The self-diffusivity $\overline{D}$ quantifies the random motion of a species in a mixture in the absence of a concentration gradient, and is described by Einstein's expression for Brownian motion.[26]

A MFI unit cell contains six physisorption sites which significantly differ in connectivity, vide Figure 1.[32] The β sites reside at the channel intersections and are connected with 4 α neighbors. The α sites, in turn, are situated in the channels and are connected to two β sites only.

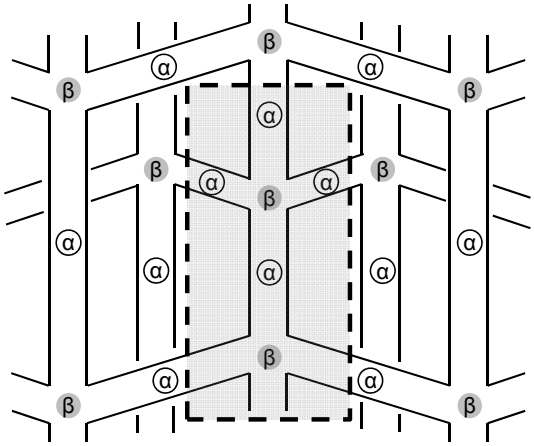

Figure 1 – Schematic representation of the MFI framework with indication of the unit cell (dashed line), the bridge physisorption sites (α) and intersection physisorption sites (β).

The incorporation of aluminium atoms in the zeolite leads to a stronger physisorption step and, consequently, a longer residence time on those sites. The latter are assumed to reside at the intersections only and are denoted as β_s from now on.[26] The other, non-reactive intersection sites are denoted as β_w. Introduction of the mean field theory which neglects any correlation between successive hops between the physisorption sites, yields an expression for the self-diffusivity at a given occupancy derived from simple connectivity rules and a global site balance.[33]

$$\overline{D}^{\mathrm{MFT}} = \overline{D}_0^0 A\left(\frac{B}{C}\right) \tag{10}$$

With

$$A = \frac{\lambda f + 2 - f}{2}$$

$$B = 2\left(1-\theta_\alpha\right)\left[\left(1-f\right)\theta_{\beta_w} + \frac{f}{\lambda}\theta_{\beta_s}\right] + 4\theta_\alpha\left[\left(1-f\right)\left(1-\theta_{\beta_w}\right) + f\left(1-\theta_{\beta_s}\right)\right]$$

$$C = \frac{2\left(1-\theta_\alpha\right)\left[\left(1-f\right)\theta_{\beta_w} + \frac{f}{\lambda}\theta_{\beta_s}\right]}{\left(1-f\right)\left(1-\theta_{\beta_w}\right) + f\left(1-\theta_{\beta_s}\right)} + \frac{4\theta_\alpha\left[\left(1-f\right)\left(1-\theta_{\beta_w}\right) + \frac{f}{\lambda}\left(1-\theta_{\beta_s}\right)\right]}{1-\theta_\alpha}$$

In Eqn. 10, $\overline{D}_0^0$ represents the self-diffusivity at zero occupancy through a MFI crystallite without any strong physisorption sites present. Heterogeneity in physisorption strength among the different sites is accounted for via *f*, i.e., the fraction of strong physisorption sites, and λ which is the ratio of the average residence times on strong and weak physisorption sites. The residence times follow an Arrhenius-type relationship with the corresponding standard physisorption enthalpies,[34] which, in turn, are used for the calculation of λ.

$$\lambda = \mathrm{e}^{-\frac{\Delta H_{\mathrm{phys}}^{0,\mathrm{s}} - \Delta H_{\mathrm{phys}}^{0,\mathrm{w}}}{RT}} \tag{11}$$

The mean field approximation was found suitable at low to medium occupancies. However, stronger deviations between model and experiment emerged in case of higher

occupancies and frameworks with a poor site connectivity, such as MFI. The backward hop to the source site is more likely to occur than transfer towards another site resulting in a highly correlated jump frequency.[26,32] The corrected diffusivity is, by definition, devoid from any intermolecular correlation and is a much better approximation by the mean field theory via Eqn. 10:

$$\overline{D}^{\mathrm{MFT}} \approx \tilde{D}^{\mathrm{s}} \tag{12}$$

2.3 Hydrocracking single-event microkinetics

Alkane hydrocracking consists of only a limited amount of elementary step types. After physisorption, described via a single-site Langmuir isotherm,[35,36] alkanes are converted into alkenes on a metal site. Unlike other metals, platinum is ideally suited for fast dehydrogenation and, therefore, it is reasonable to assume that 'ideal hydrocracking' conditions, implying quasi-equilibrium of the (de)hydrogenation reactions, are established.[37,38] Assuming equilibrium for the (de)protonation reactions as well leads to the general expression for the rate of an elementary isomerization or cracking step:[24]

$$r = \frac{C_{\mathrm{sat}} C_{\mathrm{acid}} K_{\mathrm{pro}} K_{\mathrm{deh}} K_{\mathrm{phy}}^{\mathrm{L}} p_{\mathrm{P}} p_{\mathrm{H_2}}^{-1}}{\left(1+\sum_{\mathrm{npar}} K_{\mathrm{phy}}^{\mathrm{L}} p_{\mathrm{P}}\right)\left(1+\frac{\sum_{\mathrm{ncar}} C_{\mathrm{sat}} K_{\mathrm{pro}} K_{\mathrm{deh}} K_{\mathrm{phy}}^{\mathrm{L}} p_{\mathrm{P}} p_{\mathrm{H_2}}^{-1}}{1+\sum_{\mathrm{npar}} K_{\mathrm{phy}}^{\mathrm{L}} p_{\mathrm{P}}}\right)} n_e \tilde{k} \tag{13}$$

Where p_P equals the partial pressure of the alkane, C_{sat} the saturation concentration of the alkane, C_{acid} the total concentration of acid sites, K_{pro} the protonation equilibrium coefficient, K_{phy}^{L} the Langmuir physisorption coefficient determined from the linear relationship between the standard physisorption enthalpy and entropy and the sorbate carbon number,[39] and K_{deh} the dehydrogenation equilibrium coefficient determined from Benson's group contribution method.[40] The rate coefficient k is split up in the single-event rate coefficient $\tilde{k}$ which is equal for each elementary step within the corresponding reaction family, and a factor which quantifies the number of structurally indistinguishable ways the elementary step can occur. The so-called 'number of single events' factor, n_e, is calculated from the global symmetry numbers of the transition state and the reactant ion:

$$n_e = \frac{\sigma_{\mathrm{R^+}}}{\sigma_{\neq}} \tag{14}$$

The reaction families depend on the type of elementary step and the type of carbenium ion involved as reactant and product. Thybaut et al.[24] determined the single-event activation energies for 1,2-alkyl shifts, PCP-branching and β-scission and were used in this work, hence, assuming free carbenium ion chemistry.

3. Application to *n*-hexane hydrocracking

3.1 Procedures

The SEMK model described in Section 2 was validated by means of a *n*-hexane hydrocracking data set over a Pt/H-ZSM5 acquired in a Berty lab-scale CSTR setup.[41] 4.85 g of Pt/H-ZSM5 with a Si/Al ratio of 137 and an average crystallite size of 0.5 μm was crushed and sieved into pellets of approximately 500 μm, loaded in the reactor and in situ reduced with hydrogen at 673 K for 4 hours prior to reaction. Reactions were carried out at either 503 or 523 K while the pressure was varied between 1 and 3 MPa. The hydrogen-to-hydrocarbon molar ratio was varied from 50 to 100 and the space time from 98 to 430 kg s

mol^{-1}. Methane was used as an internal standard for GC analysis. The molar balance equation was considered for each reaction product:

$$F_i - F_i^0 - R_i W = 0, \quad \text{I} = 1, 2, \ldots, n\text{-}1 \tag{15}$$

The set of *n*-1 algebraic equations was solved by means of the DNSQE subroutine available at NETLIB.[42] The molar outlet flow rate of the feed component and hydrogen were calculated afterwards by means of a carbon and a hydrogen balance, respectively. The net production rate of each component was calculated from integration over the catalyst crystallite which is divided into equidistant points. The steady-state concentration profile at each point is determined from integration of the unsteady-state mass balance over a sufficient amount of time, e.g., for component *i*:

$$\frac{\partial C_i}{\partial t} = \frac{1}{r^s}\frac{\partial}{\partial r}\left(r^s D_i \frac{\partial C_i}{\partial r} \right) + R_i \tag{16}$$

Where *s* is the crystallite shape factor and is equal to either 0, 1 or 2 for respectively a slab, cylindrical and spherical geometry. The rather irregular shape of the crystallite could reasonably be approximated by a spherical geometry.[43] The transport diffusivity was calculated from the corrected diffusivity via the MS methodology, vide Section 2.1. The corrected diffusivity, in turn, was approximated by the self-diffusivity determined via the mean field theory described in Section 2.2. The pre-exponential factor and the activation energy for diffusion in the Arrhenius equation of the corrected diffusivity, Eqn. 9, were estimated via non-linear regression against the experimental data. Initial estimates were difficult to assign as, within literature, large discrepancies between the measured or modeled values for the self-diffusivities from different experimental and theoretical.[44] Nonetheless, relative differences in diffusivities between the individual alkanes were confirmed by most techniques. The measured diffusivities via Temporal Analysis of Products (TAP) were chosen as initial values as the technique is able to overcome many issues encountered during microscopic and macroscopic measurements, such as thermodynamic phenomena and carrier gas effects.[45-47]

The net production rate in Eqn. 16 was calculated using the methodology described in Section 2.3. The standard alkene protonation enthalpy for secondary carbenium ion formation quantifies the average acid strength of the catalyst and was estimated as well. Parameter estimation was carried out via a weighed sum of squares minimization using a combination of an in-house written Rosenbrock algorithm and the Levenberg-Marquardt method for final optimization.[48,49] The latter method was selected via the Ordinary Least Squares (OLS) option in ODRPACK version 2.01 available at NETLIB.[42]

3.2 Results and discussion

The overall catalyst activity was well predicted, vide Figure 2 which shows the parity diagram for the total *n*-hexane conversion. A standard alkene protonation enthalpy of -70.0 ± 0.2 kJ mol^{-1} was estimated which is in good agreement with simulation results from other zeolite topologies.[13,24] In addition, the modeled yields for 2-methylpentane and 3-methylpentane show a satisfactory agreement with the experimentally obtained results as shown in Figure 3. The difference in hydrocracking behaviour with a large-pore faujasite is also depicted. Clearly, a higher isomerization yield was obtained on the ZSM5 catalyst. However, from heavier feeds on, experimental studies showed that the latter catalyst is renowned for its excessive cracking behavior due to the immobile dibranched species,[10,17] which, in case of the *n*-hexane hydrocracking reaction network, cannot be directly transformed into propane via β-scission.

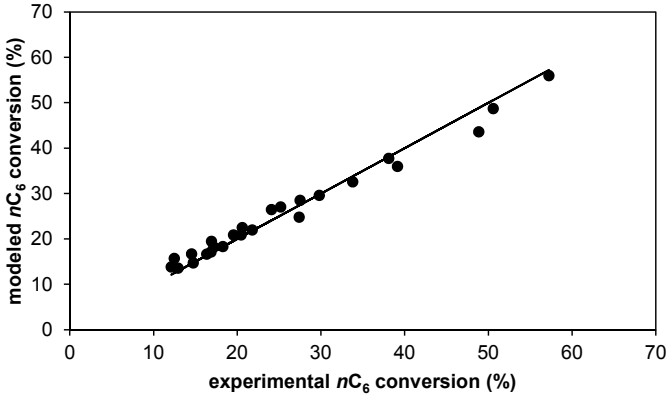

Figure 2 – Parity diagram between the modeled and the experimental *n*-hexane conversion.

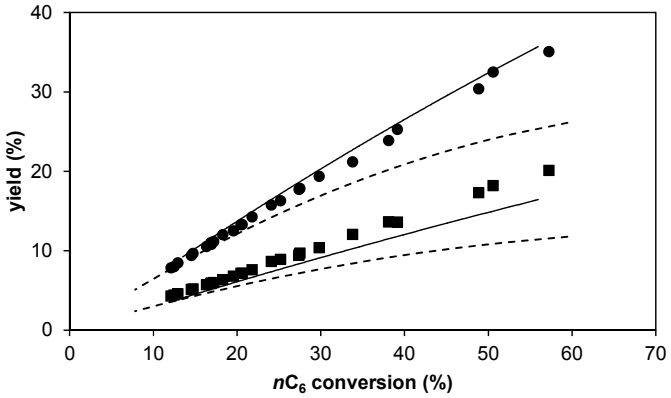

Figure 3 – Agreement between the modeled (lines) and experimental (symbol) 2-methylpentane (circles) and 3-methylpentane (squares) yield; Simulation of both yields for a faujasite catalyst (dashed lines).

A very high diffusional activation energy was attributed to both 2,2-dimethylbutane and 2,3-dimethylbutane, vide Table 1, in order to simulate their fixed position within the unit cell which, according to other works,[50,51] is restricted to the intersection sites only. The diffusional parameters of propane were also fixed throughout the parameter estimation routine as the relatively weak Van der Waals interaction with the zeolite lattice leads to a negligible contribution to the steady-state concentration profiles. The diffusivity of *n*-hexane remains substantially lower than the diffusivities of its monobranched isomers which is in line with expectations. Subtle differences in diffusion parameters between 2-methylpentane and 3-methylpentane, leading to a slightly higher diffusivity for the former alkane, confirm that mass transport is hindered to a higher extent when the branch is located more to the center of the sorbate molecule.[4,52]

Table 1 – Diffusion parameters from the Arrhenius equation for the corrected diffusivity, Eqn. 9, and the corrected diffusivity for each component in the *n*-hexane hydrocracking reaction network.

	A_D (10^{-11} m^2 s^{-1})	$E_{a,D}$ (kJ mol^{-1})	$\tilde{D}$ at 503 K (10^{-14} m^2 s^{-1})
n-hexane	5.0	12.2	270
2-methylpentane	7.0	26.2	13.3
3-methylpentane	6.9	28.3	7.88
dimethylbutane	1.0[a]	60.0[a]	0.0005
propane	5.0[a]	7.0[a]	938

[a] fixed parameter

4. Concluding remarks and future work

The SEMK model originally designed for *n*-alkane hydrocracking over large-pore faujasites was successfully extended to *n*-hexane hydrocracking over a Pt/H-ZSM5. The peculiar hydrocracking behavior of the latter zeolite could be described by incorporating simultaneous diffusion effects induced by the narrow pore size and the typical channel configuration. Diffusion through the ZSM5 zeolite was described via the Maxwell-Stefan methodology by introducing corrected and interspecies diffusivities. Both properties could be related to the corrected diffusivity at low occupancy which, in turn, was approximated by the mean field theory applied to a MFI unit cell. The net production rate of each component in the reaction network was calculated from the steady-state concentration profiles inside the catalyst crystallites. Non-linear regression analysis using a *n*-hexane hydrocracking data set resulted in a satisfactory fit between model and experiment. In addition, the estimated diffusion parameters showed a more efficient mass transport of 2-methylpentane compared to 3-methylpentane as the branch is situated further away from the center of the molecule. As a consequence, the latter molecule resides longer inside the crystallite which results in a lower selectivity than would be expected from thermodynamic equilibrium.

In continuation of this work, the model will be validated using a *n*-octane data set to incorporate explicit cracking of the immobile dibranched species inside the crystallite. Finally, saturation effects are incorporated by extending to heavier feed components in order to approach industrial practice to a higher extent.

References

1. Marcilly CR. Where and how shape selectivity of molecular sieves operates in refining and petrochemistry catalytic processes. *Top Catal.* 2000;13(4):357-366.
2. Degnan TF. The implications of the fundamentals of shape selectivity for the development of catalysts for the petroleum and petrochemical industries. *J Catal.* 2003;216(1-2):32-46.
3. Soualah A, Lemberton JL, Pinard L, Chater M, Magnoux P, Mojord K. Hydroisomerization of long-chain n-alkanes on bifunctional Pt/zeolite catalysts: Effect of the zeolite structure on the product selectivity and on the reaction mechanism. *Appl Catal a-Gen.* 2008;336(1-2):23-28.
4. Kinger G, Vinek H. n-Nonane hydroconversion on Ni and Pt containing HMFI, HMOR and HBEA. *Appl Catal a-Gen.* 2001;218(1-2):139-149.
5. Modhera BK, Chakraborty M, Parikh PA, Jasra RV. n-Hexane Hydroisomerization over Nano-Crystalline Zeolite Beta. *Petroleum Science and Technology.* 2009;27(11):1196-1208.
6. Toch K, Thybaut JW, Vandegehuchte BD, Narasimhan CSL, Domokos L, Marin GB. A Single-Event Micro Kinetic model for "ethylbenzene dealkylation/xylene isomerization" on Pt/H-ZSM-5 zeolite catalyst. *Appl Catal a-Gen.* 2012;425:130-144.
7. Wang LS, Tao LX, Xie MS, Xu GF, Huang JS, Xu YD. Dehydrogenation and Aromatization of Methane under Nonoxidizing Conditions. *Catal Lett.* 1993;21(1-2):35-41.
8. Sommer S, Melin T, Falconer JL, Noble RD. Transport of C-6 isomers through ZSM-5 zeolite membranes. *Journal of Membrane Science.* 2003;224(1-2):51-67.
9. Jacobs PA, Martens JA, Weitkamp J, Beyer HK. Shape-Selectivity Changes in High-Silica Zeolites. *Faraday Discussions.* 1981;72:353-369.
10. Martens JA, Parton R, Uytterhoeven L, Jacobs PA, Froment GF. Selective Conversion of Decane into Branched Isomers - a Comparison of Platinum/Zsm-22, Platinum/Zsm-5 and Platinum Usy Zeolite Catalysts. *Applied Catalysis.* 1991;76(1):95-116.
11. Thybaut JW, Marin GB, Baron GV, Jacobs PA, Martens JA. Alkene protonation enthalpy determination from fundamental kinetic modeling of alkane hydroconversion on Pt/H-(US)Y-zeolite. *J Catal.* 2001;202(2):324-339.
12. Martens JA, Perez-Pariente J, Jacobs PA. Isomerization and hydrocracking of n C10 - n C17 alkanes on Pt/H-Beta. *Acta Physica et Chemica Szegediensis.* 1985;31(1-2):487-495.
13. Vandegehuchte BD, Thybaut JW, Martinez A, Arribas MA, Marin GB. n-Hexadecane hydrocracking Single-Event MicroKinetics on Pt/H-beta. *Appl Catal a-Gen.* 2012;441-442:10-20.

14. Narasimhan CSL, Thybaut JW, Marin GB, et al. Kinetic modeling of pore mouth catalysis in the hydroconversion of n-octane on Pt-H-ZSM-22. *J Catal.* 2003;220(2):399-413.
15. Uguina MA, Sotelo JL, Rodriguez A, Gomez-Civicos JI, Lazaro JJ. Liquid adsorption of linear and branched paraffins onto microporous adsorbents - Influence of adsorbent structure and Si/Al molar ratio. *Separation and Purification Technology.* 2006;51(1):72-79.
16. Choudhary VR, Choudhary TV. Entrance of straight and branched chain compounds from their bulk liquid phase into H-ZSM-5 zeolite. *Chem Eng Sci.* 1997;52(20):3543-3552.
17. Gopal S, Smirniotis PG. Factors affecting isomer yield for n-heptane, hydroisomerization over as-synthesized and dealuminated zeolite catalysts loaded with platinum. *J Catal.* 2004;225(2):278-287.
18. Parton R, Uytterhoeven L, Martens JA, Jacobs PA, Froment GF. Synergism of Zsm-22 and Y-Zeolites in the Bifunctional Conversion of N-Alkanes. *Applied Catalysis.* 1991;76(1):131-142.
19. Sree SP, Dendooven J, Koranyi TI, et al. Aluminium Atomic Layer Deposition Applied to Mesoporous Zeolites for Acid Catalytic Activity Enhancement. *Catalysis Science & Technology.* 2011;1(2):218-221.
20. Thybaut JW, Choudhury IR, Denayer JF, et al. Design of Optimum Zeolite Pore System for Central Hydrocracking of Long-Chain n-Alkanes based on a Single-Event Microkinetic Model. *Top Catal.* 2009;52(9):1251-1260.
21. Choudhury IR, Hayasaka K, Thybaut JW, et al. Pt/H-ZSM-22 hydroisomerization catalysts optimization guided by Single-Event MicroKinetic modeling. *J Catal.* 2012;290:165-176.
22. Baltanas MA, Vanraemdonck KK, Froment GF, Mohedas SR. Fundamental Kinetic Modeling of Hydroisomerization and Hydrocracking on Noble-Metal-Loaded Faujasites .1. Rate Parameters for Hydroisomerization. *Ind Eng Chem Res.* 1989;28(7):899-910.
23. Svoboda GD, Vynckier E, Debrabandere B, Froment GF. Single-Event Rate Parameters for Paraffin Hydrocracking Oil a Pt/Us-Y Zeolite. *Ind Eng Chem Res.* 1995;34(11):3793-3800.
24. Thybaut JW, Narasimhan CSL, Marin GB, et al. Alkylcarbenium ion concentrations in zeolite pores during octane hydrocracking on Pt/H-USY zeolite. *Catal Lett.* 2004;94(1-2):81-88.
25. Krishna R, Wesselingh JA. Review article number 50 - The Maxwell-Stefan approach to mass transfer. *Chem Eng Sci.* 1997;52(6):861-911.
26. Coppens MO, Bell AT, Chakraborty AK. Effect of topology and molecular occupancy on self-diffusion in lattice models of zeolites - Monte-Carlo simulations. *Chem Eng Sci.* 1998;53(11):2053-2061.
27. Paschek D, Krishna R. Inter-relation between self- and jump-diffusivities in zeolites. *Chem Phys Lett.* 2001;333(3-4):278-284.
28. Mason EA, Malinauskas AP. *Gas transport in porous media: The dusty gas model*. Amsterdam, The Netherlands: Elsevier; 1983.
29. Vignes A. Diffusion in Binary Solutions - Variation of Diffusion Coefficient with Composition. *Industrial & Engineering Chemistry Fundamentals.* 1966;5(2):189-199.
30. Dubbeldam D, Snurr RQ. Recent developments in the molecular modeling of diffusion in nanoporous materials. *Molecular Simulation.* 2007;33(4-5):305-325.
31. Kapteijn F, Bakker WJW, Zheng G, Moulijn JA. Temperature- and occupancy-dependent diffusion of n-butane through a silicalite-1 membrane. *Microporous Materials.* 1994;3:227-334.
32. Trout BL, Chakraborty AK, Bell AT. Diffusion and reaction in ZSM-5 studied by dynamic Monte Carlo. *Chem Eng Sci.* 1997;52(14):2265-2276.
33. Coppens MO, Iyengar V. Testing the consistency of the Maxwell-Stefan formulation when predicting self-diffusion in zeolites with strong adsorption sites. *Nanotechnology.* 2005;16(7):S442-S448.
34. Attard G, Barnes C. *Surfaces*. New York: Oxford University Press; 2003.
35. Jolimaitre E, Tayakout-Fayolle M, Jallut C, Ragil K. Determination of mass transfer and thermodynamic properties of branched paraffins in silicalite by inverse chromatography technique. *Ind Eng Chem Res.* 2001;40(3):914-926.
36. Denayer JF, Souverijns W, Jacobs PA, Martens JA, Baron GV. High-temperature low-pressure adsorption of branched C-5-C-8 alkanes on zeolite beta, ZSM-5, ZSM-22, zeolite Y, and mordenite. *J Phys Chem B.* 1998;102(23):4588-4597.
37. Thybaut JW, Narasimhan CSL, Denayer JF, et al. Acid-metal balance of a hydrocracking catalyst: Ideal versus nonideal behavior. *Ind Eng Chem Res.* 2005;44(14):5159-5169.
38. Chavarria-Herrnandez JC, Ramfrez J, Baltanas MA. Single-event-lumped-parameter hybrid (SELPH) model for non-ideal hydrocracking of n-octane. *Catal Today.* 2008;130(2-4):455-461.
39. Arik IC, Denayer JF, Baron GV. High-temperature adsorption of n-alkanes on ZSM-5 zeolites: influence of the Si/Al ratio and the synthesis method on the low-coverage adsorption properties. *Micropor Mesopor Mat.* 2003;60(1-3):111-124.
40. Benson SW, Cruickshank FR, Golden DM, et al. Additivity Rules for Estimation of Thermochemical Properties. *Chemical Reviews.* 1969;69(3):279-324.
41. Thybaut JW, Saeys M, Marin GB. Hydrogenation kinetics of toluene on Pt/ZSM-22. *Chem Eng J.* 2002;90(1-2):117-129.
42. Netlib. http://www.netlib.org.

43. Zhu W, Malekian A, Eic M, Kapteijn F, Moulijn JA. Concentration-dependent diffusion of isobutane in silicalite-1 studied with the ZLC technique. *Chem Eng Sci.* 2004;59(18):3827-3835.
44. Karger J. Measurement of diffusion in zeolites - A never ending challenge? *Adsorption.* 2003;9(1):29-35.
45. Keipert OP, Baerns M. Determination of the intracrystalline diffusion coefficients of alkanes in H-ZSM-5 zeolite by a transient technique using the temporal-analysis-of-products (TAP) reactor. *Chem Eng Sci.* 1998;53(20):3623-3634.
46. Nijhuis TA, VandenBroeke LJP, VandeGraaf JM, Kapteijn F, Makkee M, Moulijn JA. Bridging the gap between macroscopic and NMR diffusivities. *Chem Eng Sci.* 1997;52(19):3401-3404.
47. Nijhuis TA, van den Broeke LJP, Linders MJG, et al. Measurement and modeling of the transient adsorption, desorption and diffusion processes in microporous materials. *Chem Eng Sci.* 1999;54(20):4423-4436.
48. Rosenbrock HH. An Automatic Method for Finding the Greatest or Least Value of a Function. *Computer Journal.* 1960;3(3):175-184.
49. Marquardt DW. An Algorithm for Least-Squares Estimation of Nonlinear Parameters. *Journal of the Society for Industrial and Applied Mathematics.* 1963;11(2):431-441.
50. Calero S, Smit B, Krishna R. Configurational entropy effects during sorption of hexane isomers in silicalite. *J Catal.* 2001;202(2):395-401.
51. Zhu W, Kapteijn F, van der Linden B, Moulijn JA. Equilibrium adsorption of linear and branched C-6 alkanes on silicalite-1 studied by the tapered element oscillating microbalance. *Physical Chemistry Chemical Physics.* 2001;3(9):1755-1761.
52. Webb EB, Grest GS. Influence of intracrystalline diffusion in shape selective catalytic test reactions. *Catal Lett.* 1998;56(2-3):95-104.